Comparison of 2,2′-azobis(2-amidinopropane) hydrochloride (AAPH) and 2,2′-azobis(2,4-dimethylvaleronitrile) (AMVN) as free radical initiators: a spin-trapping study

Arkadi G. Krainev*,† and Diana J. Bigelow*

Department of Biochemistry, The University of Kansas, Lawrence, Kansas 66045-2106, USA

Spin trapping with 5,5-dimethyl-1-pyrroline 1-oxide (DMPO) and its hydrophobic analogue 2,2-dimethyl-4-phenyl-2*H*-imidazole 1-oxide (DMPIO) was used to identify and to monitor the concentration of participating radical species in oxidation reactions initiated by azo compounds: water-soluble 2,2′-azobis(2-amidinopropane) hydrochloride (AAPH) and lipophilic 2,2′-azobis(2,4-dimethylvaleronitrile) (AMVN). Incubation of AAPH with spin traps in aqueous media produced alkoxyl radical spin adducts with hyperfine splitting constants being a_N = 14.62 G, $^{\beta}a_H$ = 15.29 G, $^{\gamma}a_H$ = 0.72 G and a_N = 13.46 G, $^{\beta}a_H$ = 12.53 G, for DMPO and DMPIO, respectively. In contrast, formation of AMVN-derived peroxyl radicals was detected by both direct EPR and spin trapping in DMSO (dimethylsulfoxide) solutions. In the presence of either rabbit skeletal sarcoplasmic reticulum (SR) membranes (10 g dm^{-3} of SR protein) or egg phosphatidylcholine liposomes (10 g dm^{-3} of lipid) preloaded with AMVN no spin adduct formation was observed, for both DMPO and DMPIO spin traps, indicating that AMVN-derived radical species do not escape the lipid environment. Only a small portion of AAPH-derived alkoxyl radicals was trapped by DMPIO in the presence of SR membranes. Spectral characteristics of the DMPIO spin adduct indicate its location at the lipid–water interface. At the same time, there was virtually no effect of SR on the rate of formation and steady-state level of the DMPO-spin adduct formed in the aqueous phase. From these data we suggest that the bulky cytosolic domains of the SR Ca^{2+}-ATPase protect the membrane surface from radicals generated in the bulk (aqueous) solvent. Other evidence also demonstrates different mechanisms for free radical formation by AAPH and AMVN azo-initiators.

Oxidative damage to biological tissues accompanies diseases such as cancer, ischaemia/reperfusion injury, Parkinson's disease and many other age-related dysfunctions of the organism.[1] With the current and growing interest in mechanisms of oxidative damage, azo compounds have frequently been used as convenient free radical initiators.[2] Hydrophilic 2,2′-azobis(2-amidinopropane) hydrochloride (AAPH) has been used to generate radicals in the aqueous region, while lipophilic 2,2′-azobis(2,4-dimethylvaleronitrile) (AMVN), which partitioned into the lipid region of the membrane, has been employed to initiate the oxidation process in a lipophilic environment.

The mechanism of free radical generation upon mild thermal decomposition of azo-initiators can be presented by reactions (1)–(3).[3]

$$\mathrm{R{-}N{=}N{-}R} \xrightarrow{k_1} \underbrace{[\mathrm{N_2 + 2R^{\bullet}}]}_{\text{cage}} \xrightarrow[\text{(collapse)}]{1-e} \mathrm{R{-}R} \qquad (1)$$

$$\xrightarrow[\text{(diffusion)}]{e} 2\mathrm{R}^{\bullet} \qquad (2)$$

$$\mathrm{R}^{\bullet} + \mathrm{O_2} \xrightarrow{k_3} \mathrm{ROO}^{\bullet} \qquad (3)$$

The rate of free radical initiation (R_i) is described by eqn. (4), where e is the efficiency of radical initiation.

$$R_i = 2ek_1[\mathrm{R{-}N{=}N{-}R}] \qquad (4)$$

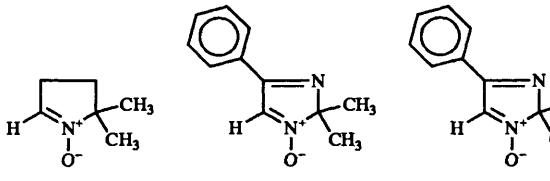

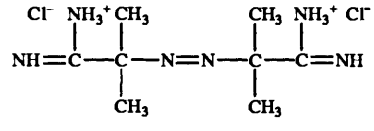

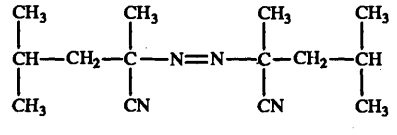

Owing to the low value of k_1 (*ca.* 10^{-7}–10^{-6} s^{-1}) and a near diffusion-controlled value of k_3 (*ca.* 10^9 dm^3 mol^{-1} s^{-1}), a constant rate of peroxyl radical (ROO$^{\bullet}$) generation may be obtained for the first few hours if a relatively large initial amount of azo compound is used, *e.g.* 10–100 mmol dm^{-3} [reactions (1)–(3)].

$$2\,\mathrm{ROO}^{\bullet} \xrightarrow{k_5} \mathrm{O_2} + 2\,\mathrm{RO}^{\bullet} \qquad (5)$$

The bimolecular self-decay constants (k_5) for some tertiary

† Postdoctoral Fellow of Marion Merrell Dow Foundation. On leave from the Biophysical Group, Institute of Chemical Kinetics and Combustion, Novosibirsk, 630090, Russia.

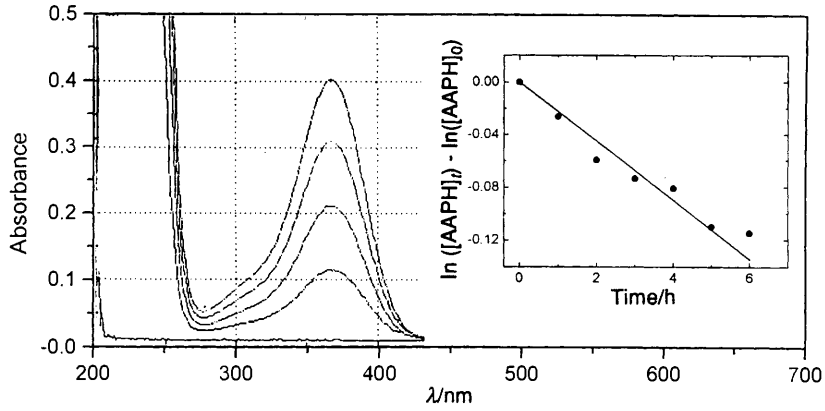

Fig. 1 The absorption spectra, from least to most intense, of 0, 5, 10, 15 and 20 mmol dm^{-3} AAPH in 10 mmol dm^{-3} potassium phosphate (pH 7.2)–100 mmol dm^{-3} KCl buffer at 22 °C. Inset: semi-log plot of AAPH decomposition; $[AAPH]_0$ and $[AAPH]_t$ denote the initial AAPH concentration and the concentration of AAPH at time t, respectively.

peroxyl radicals in water have been reported to be less than *ca.* 10^5 dm^3 mol^{-1} s^{-1}, compared with $k_5 \geqslant 1$–4×10^9 dm^3 mol^{-1} s^{-1} for a series of primary and secondary peroxyl radicals.[4] Thus it has been widely accepted that thermal decomposition of AAPH produces tertiary peroxyl radicals when employed in aqueous solutions. Although the contribution of reaction (5) to the mechanism of free radical production for different azo-initiators has been investigated in organic solvents,[5] little data is available for the water-soluble AAPH.

The chemistry of peroxyl radicals in biological experiments may be more complex, where peroxyl radicals derived from reaction (3) may interact not only with proposed target molecules, such as protein side chains, unsaturated fatty acids or antioxidants, but with other reactive oxygen species present [reactions (7), (8)]. In addition some tertiary alkoxyl radicals have been shown to undergo β-fragmentation to produce alkyl radicals [reaction (6)].[4c] The participation of reactions (6)–(8) in the oxidation mechanism of AAPH or AMVN has not been addressed either in aqueous or lipid phases. The commonly employed method of assaying oxygen consumption during oxidation will not accurately solve this question due to possible recycling of oxygen through reactions (3) and (5)–(8).

$$R^1R^2R^3CO^{\bullet} \xrightarrow{k_6} R^{1\bullet} + R^2R^3C{=}O \qquad (6)$$

$$ROO^{\bullet} + R'OO^{\bullet} \xrightarrow{k_7} O_2 + RO^{\bullet} + R'O^{\bullet} \qquad (7)$$

$$ROO^{\bullet} + O_2^{\bullet -} + H^+ \xrightarrow{k_8} ROOH + O_2 \qquad (8)$$

Therefore, we have employed the EPR spin-trapping technique[6] in order to identify and to monitor the concentration of participating radical species in the oxidation reactions initiated by AAPH and AMVN azo compounds in both water and lipid phases. We have used 5,5-dimethyl-1-pyrroline 1-oxide (DMPO)‡ as a water-soluble spin trap and 2,2-dimethyl-4-phenyl-2*H*-imidazole 1-oxide (DMPIO) as an amphiphilic spin trap which has been shown by EPR and NMR methods to be located at the water–lipid interface.[7] However, since the highly lipophilic DMPO analogue, 2-methyl-2-nonyl-4-phenyl-2*H*-imidazole 1-oxide (MNPIO), has been reported to have a limited spin trapping ability,[7a,8] we instead chose another lipophilic spin trap, α-phenyl-*N*-*tert*-butylnitrone [PhCH=N(O)Bu^t, PBN], which resides deep in the lipid bilayer.[9] We find spin-trapping to be informative and capable of providing new data on the mechanisms of azo-initiator-driven oxidation in biological systems. As an example we have documented the species and the time course of AAPH- and AMVN-generated free radicals in the presence of phospholipid vesicles and rabbit skeletal sarcoplasmic reticulum (SR) membranes.

‡ IUPAC-recommended name: 2,2-dimethyl-3,4-dihydro-2*H*-pyrrole 1-oxide.

Results

Thermal decomposition of AAPH and AMVN azo-initiators

Extinction coefficients for AAPH and AMVN were determined in order to measure their respective rate constants of thermal decomposition. For example, Fig. 1 shows the spectrum of AAPH in 10 mmol dm^{-3} potassium phosphate (pH 7.2)–100 mmol dm^{-3} KCl buffer (buffer B); the molar extinction coefficient is $\varepsilon_{367} = 19.7 (\pm 0.2)$ dm^3 mol^{-1} cm^{-1}. Spectra taken at 1 h intervals over several hours (22 °C) were found to be unchanged in shape and spectral maxima, but decreased in intensity with a single exponential decay (Fig. 1, inset). This decay was attributed to decomposition of the R–N=N–R chromophoric group. From this data the rate constant (k_1) of thermal decomposition of AAPH at 22 °C was estimated as 7.93 (± 0.49) $\times$ 10^{-6} s^{-1}. To facilitate comparison of rate constants for AAPH and AMVN, experiments were also performed in 10 mmol dm^{-3} potassium phosphate (pH 7.2)–100 mmol dm^{-3} KCl buffer containing 50 vol% acetonitrile (medium A), in which both azo compounds were soluble. AAPH and AMVN have UV spectral maxima at 368 and 345 nm, respectively [$\varepsilon_{368} = 21.9 (\pm 0.4)$ and $\varepsilon_{345} = 20.9 (\pm 1.5)$ mol^{-1} dm^3 cm^{-1}], in medium A. The rate constants for the decomposition of AAPH and AMVN in medium A at 22 °C were found to be 1.59 (± 0.1) $\times$ 10^{-5} and 2.39 (± 0.36) $\times$ 10^{-5} s^{-1}, respectively. The solvent dependency of these decay rates is illustrated by the two-fold lower rate for AAPH in buffer B relative to that in medium A.

Spin trapping with DMPO

Fig. 2(*a*) shows a typical EPR spectrum observed when incubating DMPO spin trap with AAPH in buffer B. However, one visible γ-splitting of 0.72 G has been resolved in this spectrum when using low modulation amplitude (0.1 G) and microwave power (2 mW). This observation is in agreement with properties of all oxyl DMPO spin adducts, having one relatively large γ-splitting.[6e] Other hyperfine coupling constants were obtained by computer simulation of experimental spectra taking into account the presence of unresolved γ-splittings[6d] in the DMPO spin adducts and are listed in Table 1. The spectra shown represent single radical species; no spectral contribution from other radical spin adducts was detected. To assign properly this spin adduct we obtained its EPR spectra in different

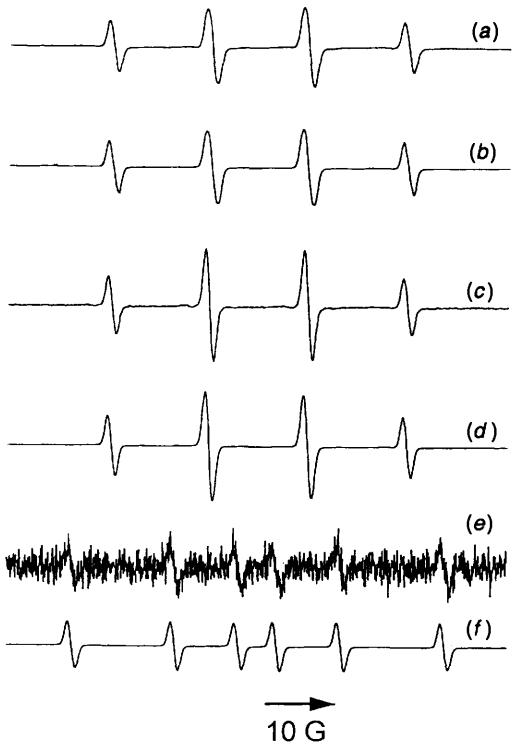

Fig. 2 EPR spectra of DMPO–AAPH spin adducts. (*a*) DMPO–'OR(AAPH) spin adduct observed (spectrometer gain 1.25×10^5, 1 h after mixing of 50 mmol dm^{-3} DMPO and 75 mmol dm^{-3} AAPH) shown with the corresponding (*b*) simulated spectrum; (*c*) DMPO–'OH spin adduct observed [spectrometer gain 5×10^4, 2.5 min after mixing of 50 mmol dm^{-3} DMPO, 1 mmol dm^{-3} H_2O_2 and 0.2 mmol dm^{-3} $FeSO_4$ (Fenton reagent)] shown with the corresponding (*d*) simulated spectrum; and (*e*) DMPO–'R(AAPH) spin adduct observed (spectrometer gain 1.25×10^5, 300 scans, 1 h after mixing of 50 mmol dm^{-3} DMPO and 75 mmol dm^{-3} AAPH; reagents were dissolved in buffer equilibrated with argon) shown with the corresponding (*f*) simulated spectrum. All samples but (*e*) were mixed in air-saturated 10 mmol dm^{-3} potassium phosphate (pH 7.2)–100 mmol dm^{-3} KCl buffer and incubated at room temp. Parameters of simulated spectra are shown in Table 1.

organic solvents;[6,10] on the basis of spectral parameters reported for a series of other similar radicals[6c,10b] this DMPO spin adduct was assigned as the AAPH-derived alkoxyl radical adduct DMPO–'OR(AAPH). We note that, consistent with the chemical structure of AAPH, the hyperfine splitting constants obtained for DMPO–'OR(AAPH) correspond most closely to those of DMPO adducts with trapped tertiary-carbon oxyl radicals (for example, compare with *tert*-butyl oxyl adducts which are also listed in Table 1).

It should be noted, however, that the spectrum of the DMPO–'OR(AAPH) spin adduct [Fig. 2(*a*)] looks remarkably similar to that of DMPO–'OH, although the measured peak-to-peak intensities for DMPO–'OR(AAPH) do not correspond to the 1:2:2:1 ratio characteristic for DMPO–'OH[10a,b] [Fig. 2(*c*)]. Line widths and individual hyperfine splitting constants derived from simulations also reveal small but significant differences (Table 1). Other considerations have allowed us to establish the unique character of the DMPO–'OR(AAPH) spin adduct. (i) 'OH ⟶ 'CH_3 conversion test: if 10 vol% dimethyl sulfoxide (DMSO) was present in the 'OH-generating Fenton system, the distinct six line DMPO–'CH_3 spectrum appeared[10c] (a_N = 16.1 G, $^{\beta}a_H$ = 23.0 G) instead of the spectrum shown in Fig. 2(*c*). However, the spectrum recorded for DMPO and AAPH in the presence of DMSO showed only slight differences relative to the DMPO–'OR(AAPH) spectrum in buffer B consistent with solvent effects[6c] (Table 1). (ii) Sensitivity to oxygen: if oxygen was removed from the reaction mixture, the formation of the DMPO–'OR(AAPH) was inhibited and the spectrum of the carbon-centred DMPO–'R adduct (a_N = 15.45 G, $^{\beta}a_H$ = 25.1 G) appeared [Fig. 2(*e*)]; the same observations have been previously reported[5b,10d] consistent with the mechanism of azo-compound decomposition [reactions (1)–(3)]. In contrast, the formation of the DMPO–'OH spin adduct was not influenced by the absence of oxygen.

In contrast to AAPH, the incubation of AMVN with DMPO in DMSO–buffer mixture produced a complex spectrum consisting of two different species [Fig. 3(*a*), Table 1]. On the basis of hyperfine coupling constants in organic solvents[10a,11] the radical adducts were assigned as the AMVN-derived peroxyl radical [DMPO–'OOR(AMVN); 69% of the measured integral intensity] and the AMVN-derived alkoxyl radical [DMPO–'OR(AMVN); 31% of the measured integral intensity]. Again, the formation of the 'OH species in this system can be completely ruled out, since in the presence of DMSO all 'OH radicals are effectively trapped (see 'OH ⟶ 'CH_3 conversion test above). In contrast, no alkoxyl radical adduct formation was detected in medium A; parameters of the DMPO–'OOR(AMVN) adduct in this solvent are listed in Table 1.

The difference in the ability of AAPH and AMVN to produce stable peroxyl radicals was further demonstrated by direct EPR measurements of these radical species. A broad-line singlet (g = 2.016) with 5.5 G peak-to-peak linewidth was observed when incubating 0.12 mol dm^{-3} AMVN in DMSO for 30 min at room temperature. The g value of 2.016 and the lack of power saturation (in 10–30 mW range) are characteristic for peroxyl free radicals that are stable at room temperature.[4a] On the other hand, no EPR signal was observed for AAPH in 0.001–0.5 mol dm^{-3} concentration range in any of the solvent systems used in the current study. Considering the sensitivity of our EPR measurements, (*i.e.* accumulation of several hundred EPR spectra within 30 min) we estimate that the steady-state concentration of any AAPH-derived peroxyl radicals must be lower than 1×10^{-9} mol dm^{-3}.

The kinetics and efficiency of spin trapping are known to be sensitive to the nature of the reaction solvent.[6] Solvent molecules may compete with DMPO molecules in the reaction (9), or, alternatively, may protect spin traps and spin adducts

$$\text{ROO}^{\bullet}/\text{RO}^{\bullet} + \text{DMPO} \xrightarrow{k_9} \text{DMPO spin adducts} \quad (9)$$

from being destroyed by active radical species (ROO'/RO') present in our reaction system [reaction (10)]. For example, we

$$\text{DMPO/DMPO spin adducts} \xrightarrow{\text{radical species}} \text{non-paramagnetic products} \quad (10)$$

find that the rate of formation and steady-state intensity of the DMPO–'OR(AAPH) spectrum was suppressed by 70% in 10 mmol dm^{-3} MOPS (pH 7.2)–110 mmol dm^{-3} KCl buffer in comparison with buffer B (data not shown). On the other hand, inclusion of 10 vol% DMSO in buffer B increased the rate of formation and intensity of the DMPO–'OR(AAPH) spectrum (compared below in Figs. 6 and 7). This could be explained by the different interference of MOPS and DMSO molecules in reactions (9) and (10). However, we cannot rule out the other possible solvent effects caused by MOPS and DMSO on this reaction system.

In contrast, we did not observe significant variations in either rate or extent of formation of the DMPO–'OR(AAPH) adduct by changing the pH of the buffer B from 6.2 to 8.2 and the KCl concentration from 0.1 to 0.5 mol dm^{-3}. In our experiments, we have employed three standard conditions: medium A (50 vol% acetonitrile, to compare AAPH and AMVN in the same

Table 1 Parameters of simulated and experimental EPR spectra of DMPO spin adducts[a]

Spin adduct	Solvent	Linewidth/G[b]	Hyperfine splitting constants/G				Ref.
			a_N	$^{\beta}a_H$	$^{\gamma 1}a_H$	$^{\gamma 2}a_H$	
DMPO–•OR(AAPH)	Buffer	0.78 (1/4)	14.62	15.29	0.72	0.42[c]	Fig. 1(*b*)
DMPO–•OR(AAPH)	Buffer–DMSO (9:1)	0.78 (1/4)	14.86	14.47	0.70	0.52[c]	This work
DMPO–•OH	Water	0.58 (1/4)	14.99	14.58	Set[d]		Fig. 1(*d*)
DMPO–•OH	Buffer	0.57 (1/4)	14.94	14.88	Set[d]		This work
DMPO–•R (carbon-centred)	Buffer	0.72 (1/4)	15.45	25.10	0.60	0.40	Fig. 1(*f*)
DMPO–•OR(AAPH)	CH_3Cl extract	1.91 (1/4)	13.10	9.10	2.40	1.50	This work
DMPO–•OR(AAPH)	CH_3CN	1.85 (1/4)	13.70	11.60	3.70	1.50	This work
DMPO–•OR(Bu^t)	Buffer (pH 6.4)	0.68 (1/1)	14.85	16.40	—	—	10(*b*)
DMPO–•OR(Bu^t)	CH_3Cl	—	13.67	9.71	1.61	—	6(*c*)
DMPO–•OR(Bu^t)	CH_3CN	—	13.54	10.71	1.35	—	6(*c*)
DMPO–•OOR(AMVN)	Buffer–DMSO (1:9)	0.89 (1/1)	13.33	7.88	1.67	0.67	Fig. 3(*c*)
DMPO–•OR(AMVN)	Buffer–DMSO (1:9)	0.89 (1/1)	12.85	11.70	2.10	0.70	Fig. 3(*d*)
DMPO–•OOR(AMVN)	Buffer–CH_3CN (1:1)	1.11 (1/1)	13.88	8.90	1.50	0.50	This work
DMPO–•OOR(Bu^t)	Toluene	—	12.72	9.36	1.44	—	11(*a*)
DMPO–•OOR(Bu^t)	Buffer (pH 7.4)	—	14.50	10.50	1.50	—	11(*b*)

[a] The hyperfine splittings are means (±0.01 G; ±0.02 G for organic solvents) of simulation parameters for 3–4 experimental spectra. [b] Peak-to-peak linewidth (in G), numbers in parentheses show relative contribution of Lorentzian and Gaussian lineshape in simulated spectra. [c] The same line shape could be obtained using the following set of γ-splitting constants, modified from ref. 6(*d*) [in G: 0.224 (2 CH_3, C5), 0.72 (H, C3), 0.229 (H, C4), 0.135 (2 H, C3, C4)] and a linewidth of 0.5 G. [d] A set of γ-splitting constants for DMPO–•OH spin adduct is taken from ref. 6(*d*) [in G: 0.224 (2 CH_3, C5), 0.370 (H, C3), 0.229 (H, C4), 0.135 (2 H, C3, C4)].

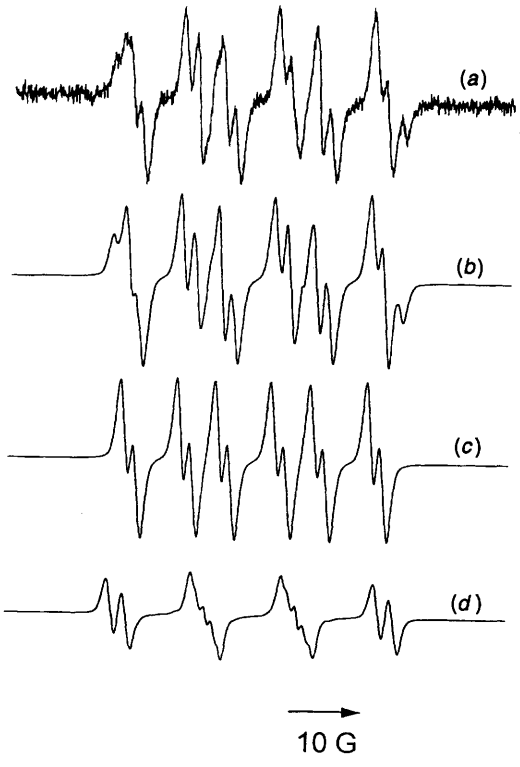

Fig. 3 EPR spectra of DMPO–AMVN spin adducts. (*a*) Complex spectrum observed (spectrometer gain 1.25×10^5, 300 scans) 1 h after mixing of 50 mmol dm^{-3} DMPO and 25 mmol dm^{-3} AMVN in 90 vol% DMSO shown with the corresponding (*b*) composite simulated spectrum of (*c*) + (*d*); (*c*) simulated spectrum of DMPO–•OOR-(AMVN), mole ratio 0.69; (*d*) simulated spectrum of DMPO–•OR(AMVN), mole ratio 0.31. Parameters of simulated spectra are shown in Table 1.

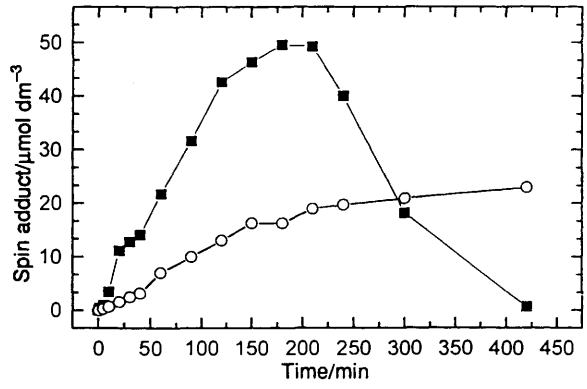

Fig. 4 The time-courses of DMPO–•OR(AAPH) (■) and DMPO–•OOR(AMVN) (○) spin adducts accumulation in the presence of 50 mmol dm^{-3} DMPO and 75 mmol dm^{-3} of corresponding azo-initiator in air-saturated 10 mmol dm^{-3} potassium phosphate (pH 7.2)–100 mmol dm^{-3} KCl buffer with 50 vol% of acetonitrile. Samples were incubated at room temp. The intensity for DMPO–•OOR(AMVN) adduct was multiplied by 300.

homogeneous solvent), buffer B (close to physiological conditions) and buffer C (*i.e.* buffer B plus 10 vol% DMSO, to introduce non-polar DMPIO into aqueous solution).

The rates of spin adduct formation in the presence of azo compounds were observed to be constant (see Fig. 4 and Experimental section) for at least the first 30 min. These initial rates of spin adduct formation [d[DMPO–•O(O)R]/dt, reaction (9)] were calculated from the slopes of spin adduct accumulation as 7.24×10^{-9} and 4.93×10^{-11} mol dm^{-3} s^{-1} for DMPO–•OR(AAPH) and DMPO–•OOR(AMVN), respectively, in medium A, where both azo-initiators show single spin adduct species. After *ca.* 140 min of incubation, a steady-state level of DMPO–•OR(AAPH) spin adduct has been formed. This level was not influenced by mixing the sample with fresh air, indicating that the oxygen supply is not limited in our sample (see Experimental section).

The DMPO–•OR(AAPH) spin adduct was eventually destroyed by active radical species present in our experimental system [reaction (10), Fig. 4], in agreement with a report that extended thermolysis of azoisobutyronitrile (AIBN) in the presence of DMPO gives a non-paramagnetic double adduct R(AIBN)–DMPO–•OR(AIBN).[5b] In contrast, no decay of the DMPO–•OOR(AMVN) spin adduct was observed for at least 7 h in the same reaction system. This could be explained by either the low reactivity of AMVN-derived peroxyl radicals towards DMPO and its spin adducts or the low concentration of •OOR(AMVN) species.

Spin trapping with DMPIO

Essentially the same behaviour was observed for the DMPIO spin trap in the presence of azo-initiators, as described above for the DMPO spin trap. The representative spectra are shown in Fig. 5 and the corresponding hyperfine splitting constants are listed in Table 2. Assuming a similar chemical structure of

Table 2 Parameters of simulated EPR spectra of DMPIO spin adducts[a]

Spin adduct	Solvent	Linewidth/G[b]	Hyperfine splitting constants/G				Ref.
			a_N	$^{\beta}a_H$	$^{\gamma^1}a_H$	$^{\gamma^2}a_H$	
DMPIO–'OR(AAPH)	Buffer–DMSO (9:1)	0.90 (1/4)	13.46	12.53	—	—	Fig. 5(*b*)
DMPIO–'OH	Water–CH_3CN (4:1)	0.80 (1/4)	15.10	14.10	—	—	Fig. 5(*d*)
DMPIO–'OR(AAPH)	CH_3CN	1.85 (1/4)	12.83	12.45	—	—	This work
DMPIO–'OOR(AMVN)	CH_3CN	1.69 (1/1)	13.50	11.60	—	—	Fig. 5(*f*)
DMPIO–'OOR(AMVN)	DMSO	0.80 (2/1)	13.30	12.58	—	—	This work

[a] See footnote for Table 1. No visible γ-splittings have been detected for DMPIO spin adducts. [b] Peak-to-peak linewidth (in G), numbers in parentheses show relative contribution of Lorentzian and Gaussian lineshape in simulated spectra.

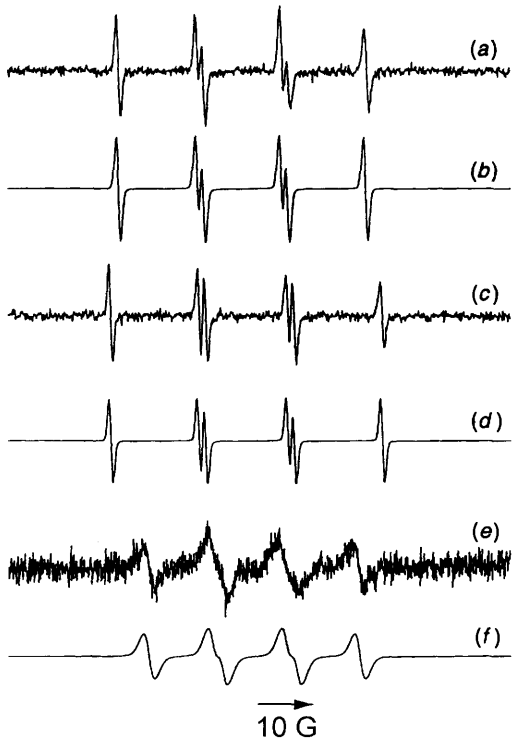

Fig. 5 EPR spectra of DMPIO spin adducts. (*a*) DMPIO–'OR(AAPH) spin adduct observed 2.5 h after mixing of 50 mmol dm^{-3} DMPIO and 75 mmol dm^{-3} AAPH in 10 vol% DMSO shown with the corresponding (*b*) simulated spectrum; (*c*) DMPIO–'OH spin adduct observed 2.5 min after mixing of 50 mmol dm^{-3} DMPIO, 1 mmol dm^{-3} H_2O_2 and 0.2 mmol dm^{-3} $FeSO_4$ (Fenton reagent) in 20 vol% acetonitrile shown with the corresponding (*d*) simulated spectrum; and (*e*) DMPIO–'OOR(AMVN) spin adduct observed (900 scans accumulated for 2 h) after mixing of 50 mmol dm^{-3} DMPIO and 75 mmol dm^{-3} AMVN in 100 vol% acetonitrile shown with corresponding (*f*) simulated spectrum. All samples were mixed in air-saturated 10 mmol dm^{-3} potassium phosphate (pH 7.2)–100 mmol dm^{-3} KCl buffer and incubated at room temp. Parameters of simulated spectra are shown in Table 2.

DMPO and DMPIO spin traps and comparing the hyperfine splitting constants obtained in different solvents we tentatively assigned AAPH- and AMVN-derived products as DMPIO–'OR(AAPH) and DMPIO–'OOR(AMVN), respectively. Note the lower a_N and a_H values for DMPIO–'O(O)R spin adducts as compared with corresponding DMPO spin adducts.

However, DMPO and DMPIO displayed significantly different time courses in the formation of AAPH-derived alkoxyl radical spin adducts (Fig. 6). From these data, the rates of spin adduct formation in reaction (9) in the presence of 10 vol% DMSO (buffer C) were calculated as 4.2×10^{-9} and 2.13×10^{-9} mol dm^{-3} s^{-1}, for DMPO and DMPIO, respectively. Also, the DMPIO–'OR(AAPH) spin adduct was less stable in any given system as compared with DMPO–'OR(AAPH). With AMVN as an initiator, DMPIO did not form any spin adducts in medium A.

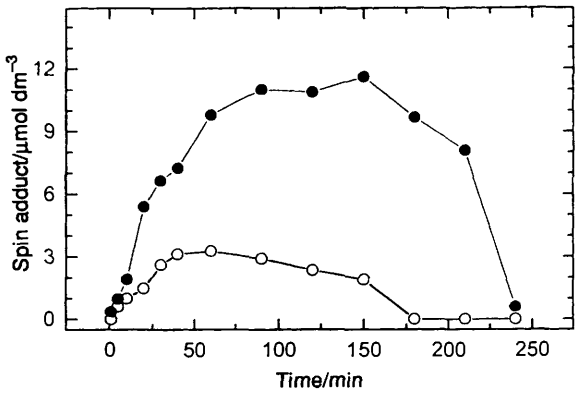

Fig. 6 The time-courses of DMPO–'OR(AAPH) (●) and DMPIO–'OR(AAPH) (○) spin adduct accumulation in the presence of 50 mmol dm^{-3} spin trap and 75 mmol dm^{-3} AAPH in air-saturated 10 mmol dm^{-3} potassium phosphate (pH 7.2)–100 mmol dm^{-3} KCl buffer with 10 vol% of DMSO. Samples were incubated at room temp.

Spin trapping in the presence of vesicular membranes

Both AAPH and AMVN have been shown to stimulate peroxidation of vesicular membrane lipids both in protein-free[2,3] and protein-containing (SR) membranes.[12] Egg phosphatidylcholine was selected as a convenient model of protein-free vesicles because of its similar fatty acid composition to SR membranes.[13] When starting with hydrophilic AAPH, no radical species other than alkoxyl radicals were detected by spin trapping in the presence of membranes.

Linewidths and hyperfine splittings for the DMPO spin adducts in the presence of membranes were identical to those in buffer B. However, the spectral characteristics of the DMPIO–'OR(AAPH) spin adduct reflect its location at the bilayer surface. For example, the spectra of the DMPIO–'OR(AAPH) spin adduct observed in the presence of SR membranes showed about 10% linewidth broadening compared with this spin adduct in the absence of membranes. Such line broadening is diagnostic of restricted motion of the DMPIO–'OR(AAPH) molecule, probably resulting from its attachment to the membrane surface. Similar observations have been reported for DMPIO and the number of different lipid-soluble spin adducts.[7-9] In contrast to the effects of SR membranes on DMPIO spin adduct dynamics, the polarity around the nitroxide group is unperturbed as evidenced by unaltered hyperfine splitting constants. Thus an aqueous environment of the nitroxide group without free tumbling in solution is consistent with attachment of the phenyl moiety of the DMPIO spin adduct to the bilayer surface.[7b]

Remarkable differences were observed between the spin-trapping abilities of DMPO and DMPIO in the presence of membranes: water-soluble DMPO more effectively competed with vesicular membranes for AAPH-derived radicals [Fig. 7(*a*)] as compared with the DMPIO spin trap, located at the lipid–water interface [Fig. 7(*b*)]. Only a small portion of alkoxyl radicals was trapped by DMPIO in the presence of SR membranes. At the same time, the addition of SR had virtually

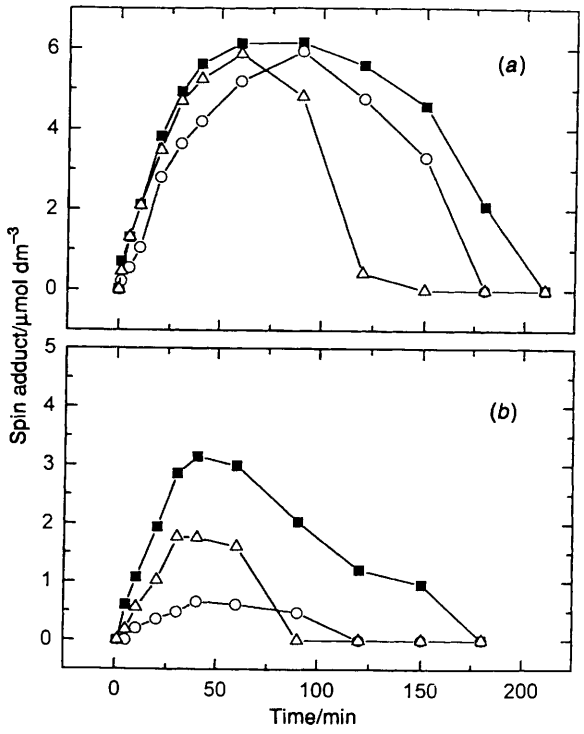

Fig. 7 The time-courses of DMPO–'OR(AAPH) (*a*) and DMPIO–'OR(AAPH) (*b*) spin adduct accumulation in the absence (■) and in the presence of either (○) SR vesicles (10 g dm^{-3} of SR protein), or (△) egg phosphatidylcholine liposomes (10 g dm^{-3} of lipid); 50 mmol dm^{-3} of corresponding spin trap and 75 mmol dm^{-3} of AAPH in air-saturated 10 mmol dm^{-3} potassium phosphate (pH 7.2)–100 mmol dm^{-3} KCl buffer with 0 (*a*) or 10 (*b*) vol% of DMSO were incubated at room temp.

no effect on the rate of formation and spin-adduct steady-state levels of DMPO–'OR(AAPH). In the presence of egg phosphatidylcholine liposomes, but not SR proteoliposomes, both DMPO- and DMPIO-spin adducts disappeared about two times faster than in the presence of AAPH alone (Fig. 7), suggesting that: (i) spin adduct decomposition is facilitated by products of AAPH-stimulated lipid peroxidation, and (ii) SR proteins prevent degradation of spin adducts, probably by diminishing the extent of lipid peroxidation.

Interestingly, when AMVN (12 mmol dm^{-3}) was incorporated into SR membranes (10 g dm^{-3} of SR protein) or egg phosphatidylcholine liposomes (10 g dm^{-3} of lipid), no spin adduct formation was observed, both for DMPO and DMPIO spin traps. This may be an indication that only minimal concentrations of AMVN-derived radical species can escape from the hydrophobic lipid environment. The production of AMVN-derived radicals within the bilayer was evidenced by an anisotropic EPR spectrum observed in the presence of 50 mmol dm^{-3} of lipid-soluble spin trap PBN (data not shown). The hyperfine splitting constants (a_N = 14.86 G, $^{\beta}a_H$ = 3.1 G) and spectral line shape were characteristic of alkyl lipid spin adducts (PBN–'L) observed during lipid peroxidation.[9] The same effect was observed in similar experiments with SR membranes.

Discussion

Spin trapping of AAPH- and AMVN-derived radicals

The aim of this study has been to examine the mechanism of azo-initiator-driven oxidation using the spin-trapping technique. This was achieved with two kinds of spin traps, DMPO and DMPIO. Both spin traps show distinct alkoxyl and peroxyl radical spin adducts in the presence of AAPH and AMVN azo-initiators (Figs. 2 and 5, Tables 1 and 2). No spin adducts of carbon-centred radicals in the presence of oxygen were observed, which could be explained by a faster rate constant of spin trapping for alkoxyl radicals than for carbon-centred radicals.[5b] For example, the ratio of these constants for 'OR(AAPH) to 'R(AAPH) trapping by DMPO estimated from intensities of corresponding spectra in Fig. 2 is *ca.* 350. This corresponds to a ratio of 550 reported[5b] for trapping *tert*-butyloxyl to *tert*-butyl radicals by the PBN spin trap.

However, there is clear evidence of different reaction mechanisms for AAPH and AMVN initiators. No peroxyl radical spin adducts have been observed employing AAPH as the initiator, which is indicative of either rapid rearrangement of the DMP(I)O peroxyl spin adducts into alkoxyl spin adducts [reaction (11)] or the higher rate of bimolecular decay for

$$\text{DMP(I)O–'OOR} \xrightarrow{k_{11}} \text{DMP(I)O–'OR} \qquad (11)$$

AAPH-derived peroxyl radicals as compared with AMVN-derived radicals [reaction (5)].

Direct EPR detection of AMVN-derived peroxyl radicals (g = 2.016) and the lack of a corresponding signal from the AAPH initiator support the last scenario. The difference in the observed properties may arise from different chemical structures of AAPH and AMVN molecules, having amidino and cyano substituents at the α-carbon, respectively. The $C(NH_2)_2^+$ group has the possibility of exerting an electron-attracting resonance effect, whereas the cyano group has strong electron-withdrawing properties.[14] Thus, it is possible that the recombination of peroxyl radicals [reaction (5)] is modulated by their electronic structure.

Another interesting observation is that the rates of azo compound decomposition measured spectrophotometrically were relatively high, for example, 1.19 × 10^{-6} mol dm^{-3} s^{-1} for AAPH (starting with 0.075 mol dm^{-3}) and 1.43 × 10^{-7} mol dm^{-3} s^{-1} for AMVN (starting with 0.006 mol dm^{-3}) compared with the corresponding rates of spin adduct formation (7.24 × 10^{-9} and 4.93 × 10^{-11} mol dm^{-3} s^{-1} for AAPH and AMVN, respectively, under the same experimental conditions). In the aqueous buffer B, the decomposition rate of AAPH was approximately two orders of magnitude greater (5.79 × 10^{-7} mol dm^{-3} s^{-1}) than that of the subsequent trapping of alkoxyl radicals by DMPO in this media (4.2 × 10^{-9} mol dm^{-3} s^{-1}). Similarly, only a small fraction of free radicals generated during thermal decomposition of these azo compounds is able to react with biological target molecules as evidenced by the low rate of malonaldehyde accumulation in the model peroxidation of SR lipids (4.33 × 10^{-13} and 1.26 × 10^{-12} mol dm^{-3} s^{-1} per mg of SR protein, for AAPH and AMVN, respectively.[12]) The major fraction of radicals is probably quenched after azo-compound decomposition and before significant diffusion can occur, *i.e.* in cage reactions,[3] or by solvent molecules.

The DMPIO spin trap when employed in a homogeneous solution had essentially the same behaviour as the DMPO spin trap. We note that most of the EPR spectra have been acquired at spectrometer settings typical for spin trapping experiments (see Experimental section). These settings result in good signal-to-noise ratios, but mask the super hyperfine structure in the EPR spectra. However, DMPIO spin adducts provide sharper lines due to the fewer number of γ-protons as compared with the DMPO structure. The study of γ-splittings in DMPO–'OR(AAPH) and DMPIO–'OR(AAPH) spin adducts and a mass spectrometry based assignment of these compounds has been recently completed in our laboratory (A. G. Krainev, T. D. Williams and D. J. Bigelow, article in preparation).

However, some differences were observed in the reactivity of these spin traps and in the stability of their corresponding spin adducts. As shown in Fig. 6, the rate of DMPO–'OR(AAPH)

spin adduct formation was about two times higher than that of DMPIO–·OR(AAPH) under the same conditions. At the same time, the steady-state concentration of DMPO–·OR(AAPH) was about three times higher than that of DMPIO–·OR(AAPH). This is expressed in eqns. (12) and (13).

$$k_9^{DMPO} = 2\,k_9^{DMPIO} \quad (12)$$

$$1.5\,k_{10}^{DMPO\text{-}{\cdot}OR(AAPH)} = k_{10}^{DMPIO\text{-}{\cdot}OR(AAPH)} \quad (13)$$

Spin trapping in the presence of vesicular membranes

The same AAPH-derived alkoxyl radical spin adducts as described above were detected in the presence of protein-containing (SR) and protein-free (egg phosphatidylcholine liposomes) phospholipid membranes, indicating no new (detectable) radical species, either in the aqueous phase or at the lipid–water interface. However, DMPO and DMPIO show remarkable differences in their spin-trapping properties in the presence of SR membranes (10 g dm^{-3} of SR protein): water-soluble DMPO more effectively competed with SR membranes for AAPH-derived peroxyl radicals [Fig. 7(*a*)] as compared with the DMPIO spin trap, located at the lipid–water interface [Fig. 7(*b*)].

These results should be interpreted in light of the following considerations: (i) AAPH-derived alkoxyl radicals are generated in the bulk solvent, where these radicals can be readily trapped by DMPO; (ii) SR membranes are densely packed with the Ca^{2+}-ATPase, an integral membrane protein, that has a large exposed cytoplasmic domain which comprises *ca.* 70% of the total enzyme mass and is elevated about 60 Å above the bilayer surface;[15] (iii) therefore, the DMPIO spin trap, being anchored to the membrane surface by its phenyl moiety,[7] is largely protected from radicals in the bulk solvent by cytoplasmic domains of the Ca^{2+}-ATPase, as evidenced by the observation that, (iv) in the presence of protein-free egg phosphatidylcholine liposomes more DMPIO–·OR(AAPH) spin adduct was formed compared with experiments done in the presence of SR membranes [Fig. 7(*b*)].

In addition to providing a physical barrier that limits the free diffusion of radical species to the lipid–water interface, the densely packed cytoplasmic domains of the Ca^{2+}-ATPase are made up of substantial numbers of amino acids that readily react with free radicals.[16] At concentrations of 10 g dm^{-3} of SR protein, the concentration of individual amino acids comprising the Ca^{2+}-ATPase sequence,[17] about 0.1 mol dm^{-3}, is sufficiently high to compete with the 0.05 mol dm^{-3} DMPIO in reaction (9). Some aromatic amino acids, for example tryptophan,[16b] react with AAPH-derived alkoxyl radicals very effectively, *i.e.* with a reaction constant close to diffusion-controlled limits. Indeed, the concentration of AAPH-derived alkoxyl radicals in the local DMPIO environment, *i.e.* at the bilayer surface, is about six times lower in the presence of SR membranes, but only about two times lower in the presence of lipid vesicles, as compared with experiment in the absence of vesicular membranes [Fig. 7(*b*)].

Another possible mechanism for decreased spin adduct formation cannot be ruled out, *i.e.* quenching by antioxidants present in SR membranes, such as α-tocopherol or dihydrolipoic acid. It has been shown[18] that these antioxidants may effectively capture free radicals on the membrane surface. In fact, the 5 min lag period observed [Fig. 7(*b*)] for DMPIO spin trapping of ·OR(AAPH) radicals in the presence of SR membranes may be attributed to the preferential reaction of radicals with antioxidants until the available antioxidant supply is consumed. This observation is consistent with the existence of a similar lag period in the development of erythrocyte haemolysis in the presence of AAPH;[18c] in that study, the extent of the lag period increased with increasing antioxidant concentrations.

Surprisingly, in the presence of phospholipid membranes preloaded with AMVN, no spin adducts were detected employing either DMPO or DMPIO spin traps. At the same time, we and others see evidence of free radical production by AMVN in phospholipid[2,3] and SR[12] membranes from the detection of the products of lipid peroxidation, *i.e.* malonaldehyde and other carbonyl compounds. This can be explained by assuming that all AMVN-derived radical species do not escape from the hydrophobic lipid environment. Indeed, when AMVN-loaded phospholipid vesicles were also preloaded with the lipid-soluble spin trap PBN, the accumulation of a lipid-PBN spin adduct was detected. Thus we emphasize the importance of a separate consideration for the chemistry of reactive oxygen species inside the hydrophobic membrane interior.

Conclusion

The EPR spin-trapping technique was found to be informative for the examination of the radicals derived from the thermal decomposition of azo compounds. In particular, we have demonstrated differences in the mechanism of AAPH and AMVN decomposition. Moreover, using spin traps of different lipophilicity, we find differences in local concentrations of AAPH-derived alkoxyl radicals in the bulk solvent and in the proximity of SR membranes. In agreement with previously reported[19] *in vivo* and *in vitro* studies, DMPO effectively captures free radicals generated in aqueous solution, acting as a potential antioxidant.

Experimental

AAPH was obtained from Eastman Kodak (Rochester, NY). AMVN was supplied from Polysciences, Inc. (Warrington, PA). The DMPIO spin trap was synthesized at The Institute of Organic Chemistry, Novosibirsk, Russia, as previously described.[8] Other reagents were of commercial grade and were supplied by Sigma (St. Louis, MO). Double-distilled ultrapure (LABCONCO Waterpro™ PS) water was used throughout for all experimental solutions.

DMPO was purified as previously described,[20] and a 5–6 mol dm^{-3} stock solution in water was stored frozen until used. DMPIO was introduced into water solutions in a small volume of DMSO. AMVN and PBN were partitioned in SR membranes according to the method previously described.[2c] Egg phosphatidylcholine (Avanti Polar Lipids, Inc., Alabaster, AL) vesicles were prepared by extrusion of multilamellar lipid-water dispersions six times through 0.6 μm COSTAR® polycarbonate membranes. To prepare lipid dispersions, an appropriate amount of lipid (and, if desired, AMVN and PBN) was introduced into a glass tube as a chloroform solution and dried under a stream of nitrogen; the water phase was added followed by ultrasonication in a bench-top BRANSON 1200 sonication bath until the dispersion became homogeneous. SR vesicles were prepared from rabbit skeletal white (fast twitch) muscle, essentially as described previously.[21] SR vesicles were stored frozen at −70 °C. For each new experiment, a small portion of SR membranes was thawed and resuspended in buffer B after additional ultracentrifugation. Lipid vesicles and SR membranes were kept on ice and used within 8 h. The thermal decomposition of azo-initiators was monitored spectrophotometrically on a Beckman DU7500 instrument.

EPR spectra were recorded on a Bruker ESP-300 E spectrometer equipped with a standard rectangular cavity ER 4102ST, operated at 9.62 GHz with 100 kHz magnetic field modulation. 50 μl (1 μl ≡ 1 mm^3) samples were mixed in Eppendorf™ tubes and transferred into a 50 μl WIRETROL® (Drummond) glass capillary and sealed with Seal-ease® (Clay Adams) at the bottom. Typical instrumental settings were as follows, if not stated otherwise: microwave power, 20 mW; modulation amplitude, 1 G; conversion time, 82 ms; time constant, 10.24 ms; gain 5×10^5; sweep width, 100 G with 2048

point resolution. These conditions are widely used in spin trapping experiments to enhance sensitivity.[6] 4-hydroxy-TEMPO was used as a standard for EPR measurements at identical spectrometer settings to estimate the concentration of spin adducts from the double-integration of spectra using the software provided by Bruker.

For the fast-scan measurements of the initial rate of spin-adduct accumulation the following automation routine was used to monitor the intensity of the spectrum's second low-field line:

1 > DEL
2 > JNS 5
3 > RACQ
4 > TP inc 1
5 > PG inc 1
6 > WAIT 27 s
7 > loop 1 30.

The spectrometer was set in the signal addition mode with the following modifications in settings: conversion time, 5 ms, time constant, 1.28 ms and sweep width, 10 G.

The simulation of EPR spectra was performed with 0.01 G increment in values of hyperfine splitting constants using the Bruker EPR Simulation Program V 1.4. Since this software does not allow automatic comparison of the result of the simulation with the experimental spectrum, the minimization was performed manually using Bruker's 'Compare' menu. The simulation was considered to be satisfactory (for review, see ref. 22) when the signal-to-noise ratio in 'Experimental minus Simulated' difference spectrum was less than two.

Acknowledgements

We would like to thank Professor V. Kagan (University of Pittsburgh, PA) for his interest in this work. This work was supported in part by Scientific Education Partnership, a Marion Merrell Dow Foundation and by an NIH grant AG 12275. The EPR spectrometer was purchased with an NSF Instrument grant, BIR 9214315.

References

1 For reviews, see (*a*) *Free Radicals and Aging*, ed. I. Emerit and B. Chance, Birkhäuser, Berlin, 1992; (*b*) R. C. Kukreja and M. L. Hess, *Cardiovasc. Res.*, 1992, **26**, 641.
2 (*a*) L. Tesoriere, M. Ciaccio, A. Bongiorno, A. Riccio, A. M. Pintaudi and M. A. Livrea, *Arch. Biochem. Biophys.*, 1993, **307**, 217; (*b*) Y. Tampo and M. Yonana, *Free Radical Biol. Med.*, 1992, **13**, 115; (*c*) A. Palozza, S. Moualla and N. I. Krinsky, *Free Radical Biol. Med.*, 1992, **13**, 127.
3 (*a*) L. R. C. Barclay, S. J. Locke, J. M. MacNeil, J. Vankessel, G. W. Burton and K. U. Ingold, *J. Am. Chem. Soc.*, 1984, **106**, 2479; (*b*) E. Niki, *Methods Enzymol.*, 1990, **186**, 100.
4 (*a*) K. U. Ingold, *Acc. Chem. Res.*, 1969, **2**, 1; (*b*) C. von Sonntag and H.-P. Schuchmann, *Angew. Chem., Int. Ed. Engl.*, 1991, **30**, 1229; (*c*) C. von Sonntag, *The Chemical Basis of Radiation Biology*, Taylor and Francis, London, 1987.
5 (*a*) K. Adamic, J. A. Howard and K. U. Ingold, *Can. J. Chem.*, 1969, **47**, 3803; (*b*) E. G. Janzen, P. H. Krygsman, D. A. Lindsay and D. L. Haire, *J. Am. Chem. Soc.*, 1990, **112**, 8279.
6 (*a*) G. R. Buettner, in *Superoxide Dismutase*, ed. L. W. Oberley, CRC, Boca Raton, FL, 1982, vol. 2, ch. 4; (*b*) E. G. Janzen and D. L. Haire, in *Advances in Free Radical Chemistry*, ed. D. D. Tanner, vol. I, JAI, London, 1990, ch. 6; (*c*) E. G. Janzen, G. A. Coulter, U. M. Oehler and J. P. Bergsma, *Can. J. Chem.*, 1982, **60**, 2725; (*d*) M. M. Mossoba, K. Makino, P. Riesz and R. C. Perkins, Jr., *J. Phys. Chem.*, 1984, **88**, 4717; (*e*) E. G. Janzen and J. I.-P. Liu, *J. Magn. Reson.*, 1973, **9**, 510.
7 (*a*) G. Strul, A. A. Frimer and L. Weiner, *J. Chem. Soc., Perkin Trans. 2*, 1993, 2057; (*b*) G. Strul, H. E. Gottlieb, A. A. Frimer and L. Weiner, *J. Chem. Soc., Perkin Trans. 2*, 1994, 1229.
8 S. I. Dikalov, I. A. Kirilyuk, I. A. Grigor'ev and L. B. Volodarsky, *Bull. Russ. Acad. Sci., Div. Chem. Sci.*, 1992, **41**, 384.
9 P. B. McCay, E. D. Lai, J. L. Poyer, C. M. DuBose and E. G. Janzen, *J. Biol. Chem.*, 1984, **259**, 2135.
10 (*a*) G. R. Buettner, *Free Radical. Biol. Med.*, 1987, **3**, 259; (*b*) W. Chamulitrat, N. Takahashi and R. P. Mason, *J. Biol. Chem.*, 1989, **264**, 7889; (c) M. K. Eberhardt and R. Colina, *J. Org. Chem.*, 1988, **53**, 1071; (*d*) M. Minetti, C. Mallozzi, G. Scorza, M. D. Scott, F. A. Kuypers and B. H. Lubin, *Arch. Biochem. Biophys.*, 1993, **302**, 233.
11 (*a*) M. J. Davis and T. F. Slater, *Biochem. J.*, 1986, **240**, 789; (*b*) P. J. Thornalley, R. J. Trotta and A. Stern, *Biochim. Biophys. Acta*, 1983, **759**, 16.
12 A. G. Krainev, R. I. Viner, C. Schöneich and D. J. Bigelow, *Biophys. J.*, 1994, **66**, A199.
13 D. Marsh, *CRC Handbook of Lipid Bilayers*, CRC, Boca Raton, FL, 1990.
14 (*a*) J. Shorter, in *The Chemistry of Amidines and Amidates*, ed. S. Paton and Z. Rappoport, Wiley, Chichester-New York-Brisbane-Toronto-Singapore, 1991, p. 689; (*b*) P. Neta, R. E. Huie, S. Mosseri, L. V. Shastri, J. P. Mittal, P. Maruthamuthu and S. Steenken, *J. Phys. Chem.*, 1989, **93**, 4099.
15 C. Toyoshima, H. Sasabe and D. L. Stokes, *Nature*, 1993, **362**, 469.
16 (*a*) E. R. Stadtman, *Annu. Rev. Biochem.*, 1993, **62**, 797; (*b*) R. T. Dean, J. V. Hunt, A. J. Grant, Y. Yamamoto and E. Niki, *Free Radical Biol. Med.*, 1991, **11**, 161.
17 C. Hidalgo, in *Membrane Fluidity in Biology*, Academic Press, New York, 1985, vol. 4, ch. 2.
18 (*a*) V. E. Kagan, E. A. Serbinova, A. Safadi, J. D. Catudioc and L. Packer, *Biochem. Biophys. Res. Commun.*, 1992, **186**, 74; (*b*) V. E. Kagan, A. Shvedova, E. Serbinova, S. Khan, C. Swanson, R. Powell and L. Packer, *Biochem. Pharmacol.*, 1992, **44**, 1637; (*c*) Y. Sato, S. Kamo, T. Takahashi and Y. Suzuki, *Biochemistry*, 1995, **34**, 8940.
19 (*a*) Y. K. Zhang, D. L. Haire, J. L. Poyer and E. G. Janzen, *Free Radical Biol. Med.*, 1993, **14**, 509; (*b*) T. Kato, K. Kojima, K. Hiramoto and K. Kikugawa, *Mutat. Res.*, 1992, **268**, 105; (*c*) C.-S. Lai, T. A. Grover and L. H. Piette, *Arch. Biochem. Biophys.*, 1973, **193**, 373.
20 G. R. Buettner and L. W. Oberley, *Biochem. Biophys. Res. Commun.*, 1978, **83**, 69.
21 J. L. Fernandez, M. Rosemblatt and C. Hidalgo, *Biochem. Biophys. Acta*, 1980, **599**, 552.
22 H. L. Vancamp and A. H. Heiss, *Magn. Reson. Rev.*, 1981, **7**, 1.

Paper 5/02678D
Received 25*th April* 1995
Accepted 5*th October* 1995